S1 Morphologies electrospun PVA/SiO_2 nanofibrous membranes

Fig. S1 shows the morphologies of electrospun PVA/SiO_2 composite nanofibrous membranes obtained using precursor solutions with different PVA contents. When the PVA content was 5 wt.%, the nanofiber surface was smooth and a small amount of spindle structure was observed. The beads structure disappeared, and the nanofiber distribution was uniform for the PVA content of 6 wt.%. When the PVA content was 7 wt.%, the diameter of the PVA/SiO_2 composite nanofibers was obviously increased and the nanofiber distribution was not uniform. The process of electrospinning involves the spinning solution forming a jet due to the effect of the electrostatic field, and the jet becomes finer and nanofibers were finally solidified on the collecting device. The process of spraying from the jet to the solidified fiber involves the interaction of the viscosity resistance of the spinning solution, the surface tension and the electric field force [1].

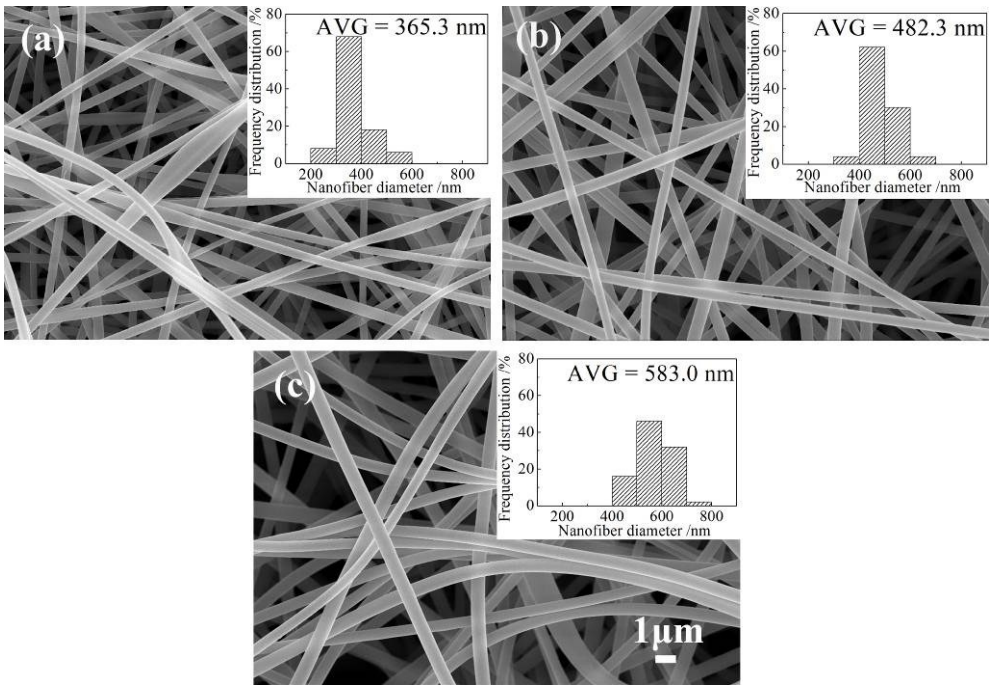

Fig. S1 Morphologies of electrospun PVA/SiO_2 composite nanofibrous membranes obtained using precursor solutions with different PVA contents: (a) 5 wt.%; (b) 6 wt.%; (c) 7 wt.%. Insets show the diameter distributions of nanofibers in membranes.

Table S1 shows the viscosity, conductivity and surface tension of the precursor solutions with different PVA contents. The viscosity of the spinning solution increased with the increasing PVA content, and the conductivity decreased, while the surface tension was almost invariable. The viscous resistance was generally characterized by viscosity, and the greater the viscosity, the greater the viscosity resistance. In the spinning process, the tensile force of the resistance to the electric field force was strong and the diameter of the nanofiber was large [2]. The lack of viscous resistance to resist the tensile force of the electric field causes the breakage of the jet when the viscosity was too low and gave rise to the formation of a beads structure. The electric field force on the jet was not uniform and because of the blocking effect of viscous resistance when the viscosity is too large, the diameter of the final collected nanofibers will be uneven and will even show entanglement. Insets of Fig. S1 show the diameter distributions of the nanofibers in the membranes. With the increase of the PVA content, the diameter distribution of the PVA/SiO_2 composite nanofiber becomes large. The average diameter increases from 365.3 to 583.0 nm, which is mainly related to the viscosity of the spinning solution [3].

Table S1 Viscosity, conductivity and surface tension of the precursor solutions with different PVA contents

PVA content /wt.%	5	6	7
Viscosity /mPa·s	135	243	440
Conductivity /μS·cm^{-1}	609	566	437
Surface tension /mN·m^{-1}	32.6	34.5	34.3

S2 Morphologies SiO_2 nanofibrous membranes

Fig. S2 shows the morphologies of electrospun SiO_2 nanofibrous membranes obtained using precursor solutions with different PVA contents. The diameter of the SiO_2 nanofibers after calcining was obviously reduced, but its morphology was basically consistent with that before calcining. The diameter shrinkage of the nanofibers was mainly due to the volatilization of the residual solvents and the decomposition of PVA during the calcination process. The inset shows the diameter distributions of the SiO_2 nanofibers in the membranes. The average diameter of the SiO_2 nanofibers increases with the increase of the PVA content, which is the same as that of the uncalcined composite nanofiber. According to the diameter distribution of the nanofibers, the spinning solution with PVA content of 6 wt.% was selected for the follow-up experiment.

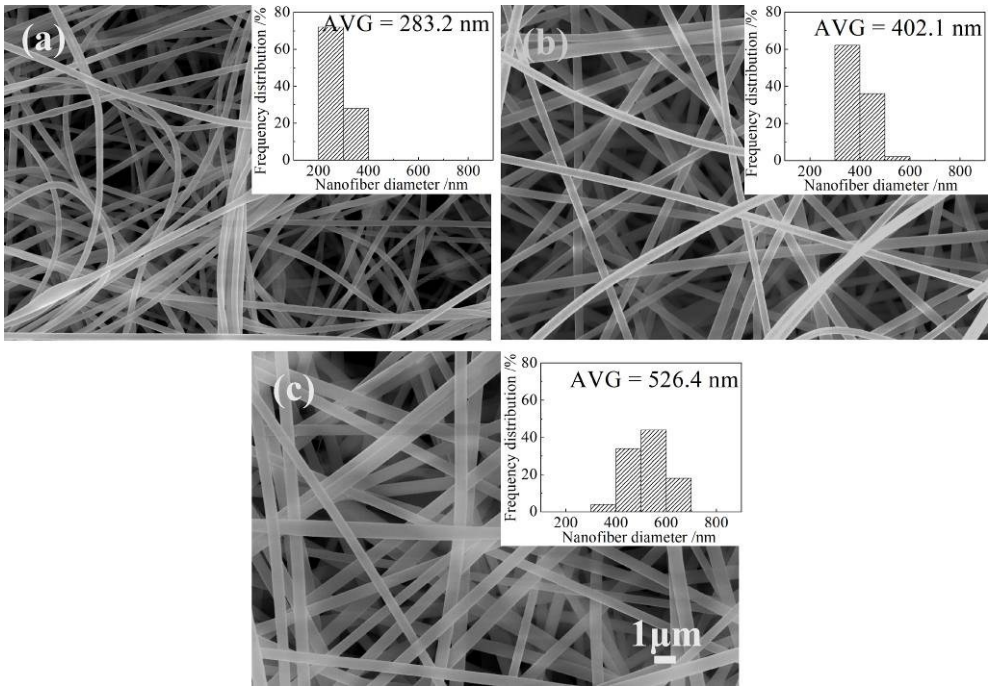

Fig. S2 Morphologies of electrospun SiO_2 nanofibrous membranes obtained using precursor solutions with different PVA contents: (a) 5 wt.%; (b) 6 wt.%; (c) 7 wt.%. Insets show diameter distributions of nanofibers in membranes.

Fig. S3 shows macro morphology of the SiO_2 nanofibrous membranes. SiO_2 nanofibrous membrane shows excellent flexibility and can be flexed arbitrarily. The flexibility was mainly because the SiO_2 was amorphous and formed by an infinite SiO4 tetrahedral network, which was consistent with some previous studies [4-5].

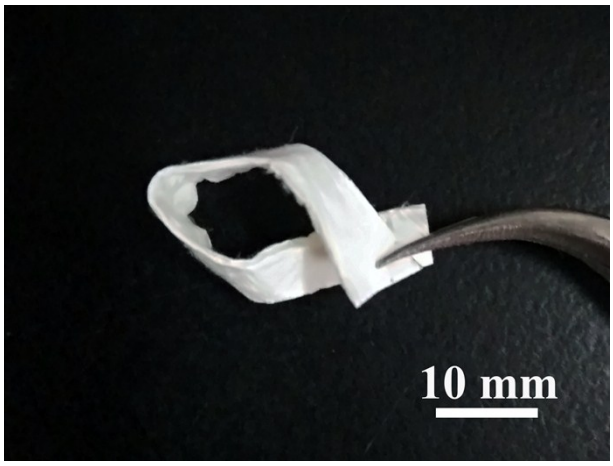

Fig. S3 Macro morphology of flexible SiO_2 nanofibrous membranes.

S3 Composition SiO_2 nanofibrous membranes

Fig. S4 shows the FT-IR spectra of the electrospun SiO_2 nanofibrous membranes before and after the calcination. In the absorption spectrum of the composite nanofibers before calcining, 3300 cm^{-1} and 2930 cm^{-1} were the characteristic peaks of PVA, representing the telescopic vibrations of the hydroxyl group (-OH) and the -CH2- on the carbon chain, respectively. The absorption peaks at 1730 cm^{-1} and 1430 cm^{-1} were caused by the vibrations of C=O and O=C-OR, respectively. The absorption peak at 1090 cm^{-1} was due to the flexural vibration of C-O-C. The abovementioned peaks basically conform to the chemical structure of PVA. In addition, the flexural vibration peaks of Si-OH appeared at 950 cm^{-1} and 790 cm^{-1}, indicating that the composite nanofibers before the calcinations contained incompletely condensed silicic acid. Symmetry stretching vibration peak of Si-O bond was observed at 519 cm^{-1}. In the FT-IR spectra of the SiO_2 nanofibrous membranes,

the characteristic peaks of silicic acid and PVA disappear. The Si-O-Si bending vibration peak appeared at 1060 cm^{-1} and the Si-O bond symmetry stretching vibration peaks appeared at 779 cm^{-1} and 512 cm^{-1}, indicating that the membrane component was SiO_2 after calcination at 600 °C for 2 h.

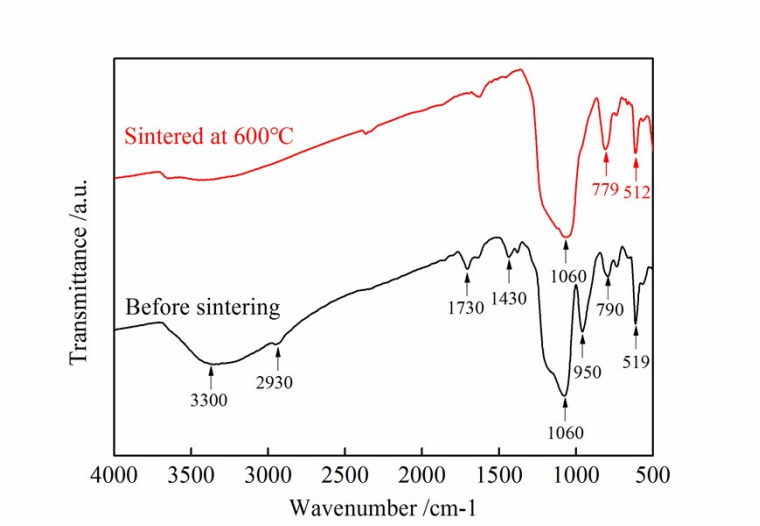

Fig. S4 FT-IR spectra of electrospun SiO_2 nanofibrous membranes before and after calcination.

S4 Morphologies of electrospun SiO_2@ZrO_2 nanofibrous membranes obtained by different centrifugal speeds

The purpose of centrifugation was to remove the residual impregnation solution that adheres to the surface and pores of the SiO_2 fibrous membranes. This can prevent the blockage of the pores that reduced the water flux and the specific surface area of the obtained membranes. Therefore, in addition to the $ZrOCl_2$ content of impregnation solutions, the centrifugation speed also affects the morphology and pore sizes of the final nanofibrous membranes. Fig. S5 shows the morphologies of the SiO_2@ZrO_2 nanofibrous membranes obtained by different centrifugal speeds in which the $ZrOCl_2$ content of the impregnation solution was 3 mol/L. When the centrifugal speed was 6000 r/min, the pore

size distribution of the SiO_2@ZrO_2 nanofibrous membrane was uniform and the average pore size was large. With the decrease of the centrifugal speed, the pore size of the SiO_2@ZrO_2 nanofibrous membranes was reduced. The impregnated solution attached to the surface and the pore of the SiO2 fiber aggregates when the centrifugal speed was 3000 r/min, and the excess ZrO_2 could partially plug the pores of the SiO_2@ZrO_2 nanofibrous membrane after calcining. The brittleness of the SiO_2@ZrO_2 nanofibrous membrane increases with the increase of the ZrO_2 shell thickness. A significant fracture of the nanofibers and the increase in the diameter of the fiber are observed. The pore size distribution of the fiber was uneven, and the average pore size was small because the excess ZrO_2 occupies the pores of the SiO_2@ZrO_2 nanofibrous membrane.

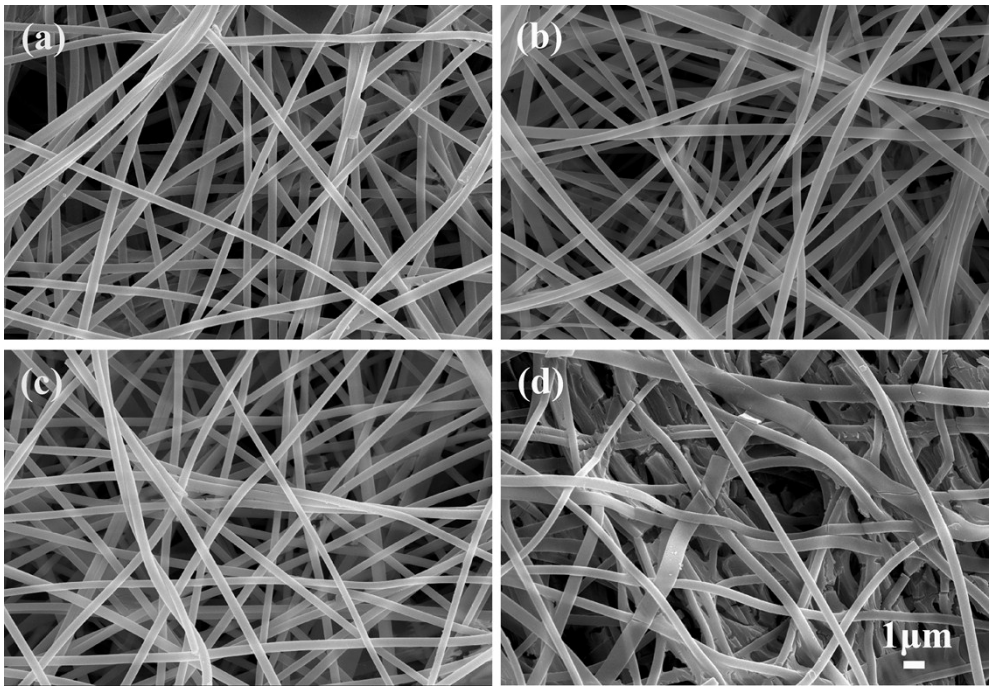

Fig. S5 Morphologies of SiO_2@ZrO_2 nanofibrous membranes obtained by different centrifugal speeds: (a) 6000 r/min; (b) 5000 r/min; (c) 4000 r/min; (d) 3000 r/min.

The pore size distributions of the SiO_2@ZrO_2 nanofibrous membranes obtained by different centrifugal speeds were calculated, as shown in Fig. S6. The insets of Fig. S6

show the distributions of the diameters of the SiO_2@ZrO_2 nanofibers in the membranes. With the decrease of the centrifugal speed, the average pore size of the fiber membrane decreased from 768.2 to 498.7 nm, and the small pore size (200-600 nm) in the pore distribution increased. When the centrifugal speed was high, the superfluous impregnated solution on the nanofiber surface can be flung out and the coaxial nanofibers with smooth surfaces and continuity can be obtained. However, when the centrifugal speed was reduced, especially at 3000 r/min, the pore size of SiO_2@ZrO_2 nanofibrous membranes was reduced greatly.

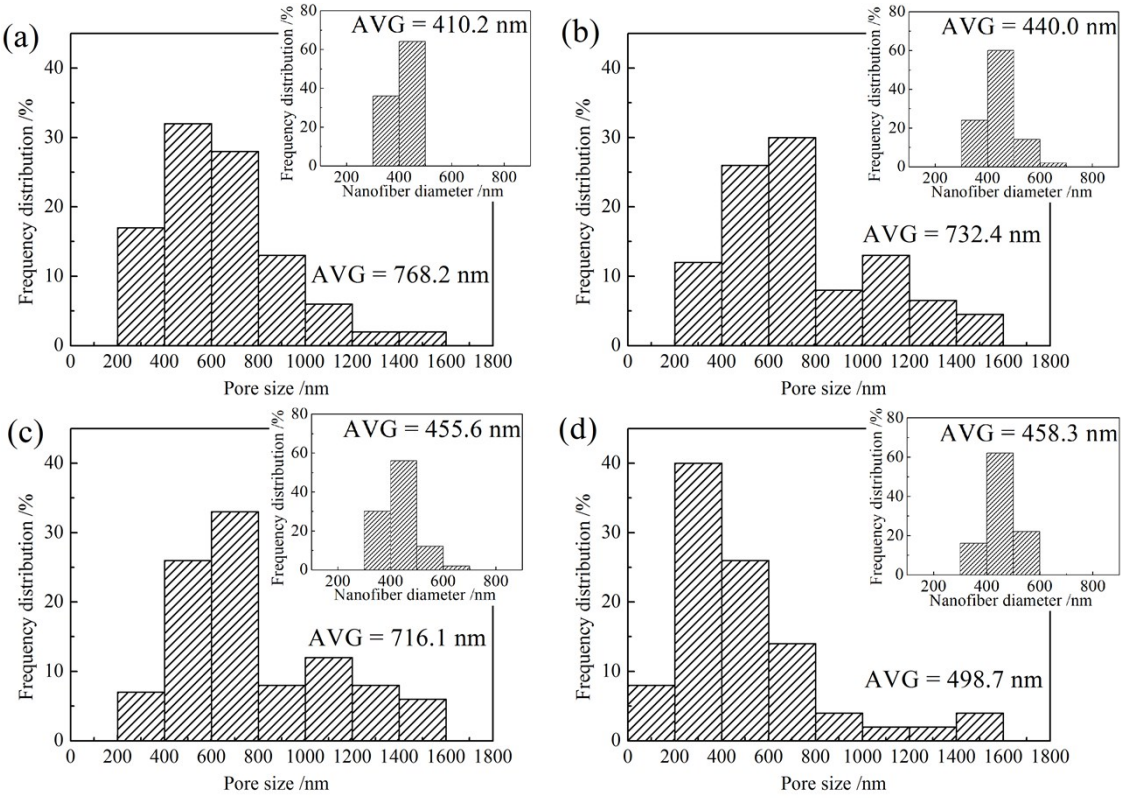

Fig. S6 Pore size distributions of SiO_2@ZrO_2 nanofibrous membranes obtained by different centrifugal speeds: (a) 6000 r/min; (b) 5000 r/min; (c) 4000 r/min; (d) 3000 r/min. Insets show the distributions of the diameters of SiO_2@ZrO_2 nanofibers in membranes.

References

[1] Y. Tang, S. Fu, K. Zhao, L. Teng, G. Xie, Fabrication of TiO_2 micro-/nano-spheres embedded in nanofibers by coaxial electrospinning, Mater. Res. Bull., 78(2016) 11-15.

[2] A.F. Spivak, Y.A. Dzenis and D.H. Reneker, A model of steady state jet in the electrospinning process, Mech. Res. Commun., 27(2000)37–42.

[3] S. Chattopadhyay, J. Saha, G. De, Electrospun anatase TiO_2 nanofibers with ordered mesoporosity, J. Mater. Chem. A 21(2014) 9029-9035.

[4] M. Guo, B. Ding, X. Li, X. Wang, J. Yu, M. Wang, Amphiphobic nanofibrous silica mats with flexible and high-heat-resistant properties[J]. J. Phy. Chem. C 114(2010)916-921.

[5] X. Wang, L. Dou, L. Yang, J. Yu, B. Ding, Hierarchical structured MnO_2@SiO_2, nanofibrous membranes with superb flexibility and enhanced catalytic performance, J. Hazard. Mater. 324(2017) 203-212.